

Comparison of Gd addition effect on the superconducting properties of FeSe_{0.5}Te_{0.5} bulks under ambient and high-pressure conditions

Manasa Manasa¹, Mohammad Azam¹, Tatiana Zajarniuk², Ryszard Diduszko³, Jan Mizeracki¹, Tomasz Cetner¹, Andrzej Morawski¹, Andrzej Wiśniewski², Shiv J. Singh^{1*}

¹*Institute of High Pressure Physics (IHPP), Polish Academy of Sciences, Sokółowska 29/37, 01-142 Warsaw, Poland*

²*Institute of Physics, Polish Academy of Sciences, aleja Lotników 32/46, 02-668 Warsaw, Poland*

³*Łukasiewicz Research Network Institute of Microelectronics and Photonics, Aleja Lotników 32/46, 02-668 Warsaw, Poland*

*Corresponding author:

Email: sjs@unipress.waw.pl

Abstract

We have prepared a series of (FeSe_{0.5}Te_{0.5} + *x*Gd) bulk samples, with *x* = 0, 0.03, 0.05, 0.07, 0.1 and 0.2, through the convenient solid-state reaction method at ambient pressure (CSP). High gas pressure and high-temperature synthesis methods (HP-HTS) are also applied to grow the parent compound (*x* = 0) and 5 wt% of Gd-added bulks. Structural, microstructural, transport and magnetic characterizations have been performed on these samples in order to draw the final conclusion. Our analysis results that the HP-HTS applied for the parent compound enhances the transition temperature (T_c) and the critical current density (J_c) with the improved sample density and intergrain connections. The lattice parameter '*c*' is increased with Gd additions, suggesting a small amount of Gd enters the tetragonal lattice of FeSe_{0.5}Te_{0.5} and the Gd interstitial sites are along the *c*-axis. A systematic decrease of the onset transition temperature T_c is observed with Gd additions, however, the calculated J_c of these Gd-added samples is almost the same as that of the parent compound prepared by CSP. It specifies that there is no improvement of the grain connections or pinning properties due to these rare earth additions. However, Gd-added FeSe_{0.5}Te_{0.5} bulks prepared by HP-HTS have revealed a slightly improved critical current density due to improved grain connections and sample density but have a lower transition temperature than that of the parent compounds.

Keywords: Superconductivity, Grain boundaries, Hot isostatic pressing, Magnetic properties, Iron-based superconductor

Introduction

The discovery of iron-based superconductors (FBS) [1] provides the second high T_c superconductors after the first high T_c cuprate superconductors [2]. Interestingly, these FBS are very rich in chemistry, and many kinds of doping have been reported [3, 4]. More than 100 compounds are available for this high T_c material that can be categorized into six families based on the crystal structure of its parent compound [5, 6, 7], and the maximum transition temperature is reached up to 58 K [8]. In all these families, FeSe belonging to the 11 family has the simplest crystal structure and depicts the critical transition temperature (T_c) of 8 K at ambient pressure [9, 10, 11]. Edge-sharing tetrahedral FeSe₄ layers are the sole layers in FeSe, and they are stacked along the c -axis. No charge storage layer exists. A structural transition from tetragonal to orthorhombic occurs at about $T_s \sim 90$ K accompanied by the nematic phase [12]. However, various kinds of doping in 11 family have been reported, such as Co, Ni, Cu, Cr at Fe sites and S, Te at Se sites, to understand the chemical pressure effect [13, 10, 14], the superconducting mechanism, and to enhance the superconducting properties. In all these doping, the substitution of Te at Se sites has enhanced the T_c value up to 15 K at ambient doping for 50% substitution [15, 16]. Furthermore, the applied pressure effect on FeSe has enhanced the transition temperature up to 36.7 K [15]. The reported upper critical field of 50 T and the critical current density of $\sim 10^4$ A/cm² (0 T, 5 K) have been obtained for the 11 family [15, 17], which also doesn't contain any harmful elements like arsenic. To enhance the superconducting properties of these materials, different kinds of methods have been applied, such as metal addition [18, 19, 20, 21], applied pressure studies, high-pressure synthesis [17], etc. by improving the grain boundaries [22].

One of the basic challenges of this 11 family is to prepare a completely pure superconducting phase due to the complicated phase diagram of FeSe [23, 10, 24, 11] which has many stable crystalline forms such as tetragonal β -Fe_xSe, hexagonal δ -Fe_xSe, orthorhombic FeSe₂, monoclinic Fe₃Se₄, and hexagonal Fe₇Se₈, in which the tetragonal phase generally exhibits superconductivity with $T_c = 8$ K [11]. During the growth process, a number of these stable phases, particularly, hexagonal δ -Fe_xSe and hexagonal Fe₇Se₈, appear along with the primary tetragonal β -Fe_xSe phase, but they lack the necessary superconducting properties. High-pressure synthesis of these materials is also not able to completely reduce the hexagonal phase but enhances the superconducting properties of Fe(Se,Te) [17]. To improve the superconducting properties of FBS, one of the most common methods at ambient pressure is the metal additions [6, 3, 18]. In this direction, many kinds of metal addition such as Pb, Sn,

Li, Ag, Potassium iodide (KI) [25, 26] *etc* have been reported [27, 18, 28, 29] and interestingly, these metal additions reduce the hexagonal phase of Fe(Se,Te) and promote the tetragonal phase formation which works well for a small amount of addition by enhancing the superconducting properties of 11 family [18].

In the case of MgB₂ superconductor [30], many transition metal additions have been reported, among which some unique properties have been observed with the rare earth (*RE*) additions. Many studies have been reported on the addition of *RE* elements and their compounds. Rare earth doping in MgB₂ such as Y, La, Dy, Ho, Nd *etc* has significantly enhanced the critical current density J_c [30]. These *RE* react with boron (B) and form impurities phases such as REB_6 and REB_4 in MgB₂ superconductors because the larger diameter of *RE* ions makes it hard to introduce them into the Mg sites in the MgB₂ lattice. However, the enhancement of critical current density and upper critical have been substantially achieved in these alloyed compounds, whereas the critical transition temperature T_c is almost unchanged. Similarly, various studies have also been reported for other superconductors, such as NbTi [31]. These studies motivated us to study and understand the superconducting properties of FeSe_{0.5}Te_{0.5} bulks with rare earth additions. Additionally, there is no report based on the rare earth addition of Fe(Se,Te) bulks, which is the main motivation of this research paper.

Here, a series of Gd-added FeSe_{0.5}Te_{0.5} bulks (FeSe_{0.5}Te_{0.5} + x Gd; $x = 0, 0.03, 0.05, 0.07, 0.1, \text{ and } 0.2$) have been prepared by the solid-state reaction method at ambient pressure, *i.e.* convenient synthesis process (CSP) and by HP-HTS. These samples are well characterized by structural, microstructure, magnetic, and transport properties to understand the rare earth addition effects on the superconducting properties of the parent compound of FeSe_{0.5}Te_{0.5}. The detailed structural and microstructural analysis depicts that the hexagonal phase is reduced completely with Gd additions and is not observed again even at high amounts of Gd additions. HP-HTS of the parent compound ($x = 0$) are very effective for the enhancement of the superconducting phase, however, the HP-HTS growth of Gd-added samples reduces the transition temperature, and a slightly improved J_c is observed due to the improved intergrain connections. Our various analyses suggest that Gd is entered the superconducting lattice and the hexagonal phase is completely reduced. However, the superconducting properties are decreased systematically with Gd additions.

Experimental details

A series of Gd additions, $\text{FeSe}_{0.5}\text{Te}_{0.5}$ ($\text{FeSe}_{0.5}\text{Te}_{0.5} + x\text{Gd}$), has been prepared by CSP at ambient pressure with $x = 0, 0.03, 0.05, 0.07, 0.1,$ and 0.2 . Basically, these samples followed a two-step process. In the first step, the starting precursors: Fe powder (99.99% purity, Alfa Aesar), Se (99.99% purity, Alfa Aesar), and Te (99.99% purity, Alfa Aesar) were mixed according to stoichiometric $\text{FeSe}_{0.5}\text{Te}_{0.5}$ composition in an agate mortar and then prepared into the pellets of 12 mm diameter. These pellets were sealed into an evacuated quartz tube, which was placed inside the furnace and heated at 600°C for 11 hours. After this step, the quartz tube was opened inside the glove box and the obtained pellets were reground. Then, we mixed Gd metal (99.9%, Alfa Aesar) with 0 wt% ($x = 0$), 3 wt% ($x = 0.03$), 5 wt% ($x = 0.05$), 7 wt% ($x = 0.07$), 10 wt% ($x = 0.10$), and 20 wt% ($x = 0.2$), and each Gd added samples were prepared at a weight of 1 gram. After the grinding process, this powder was prepared in a pellet of 12 mm diameter and sealed inside an evacuated quartz tube. Again, this prepared ampoule was heated at 600°C for 4 h inside the furnace. The final prepared pellet has a diameter of 12 mm and a 2.5 mm thickness. All synthesis processes were performed inside a high-purity argon-filled glove box. Various batches of these samples were produced under the same synthesis conditions to confirm their reproducibility. More details about the synthesis process is reported elsewhere [18, 27] and the details about the prepared bulks are listed in Table 1.

We have also prepared Gd added $\text{FeSe}_{0.5}\text{Te}_{0.5}$ bulks with the HP-HTS method, which can apply the inert gas pressure of up to 1.8 GPa inside a cylindrical chamber. This high-pressure chamber is equipped with a single zone or three zone furnace. More details are discussed elsewhere [17]. In the first step, the initial precursors Fe, Se, and Te were mixed according to the stoichiometric composition and heated in a furnace at 600°C for 11 h, as discussed above as the first step. In the second step, Gd metal is added to the prepared $\text{FeSe}_{0.5}\text{Te}_{0.5}$ after the first step and sealed inside a Ta-tube under an Ar-gas atmosphere through an ARC melter. This sealed metal tube is placed inside the pressure chamber and applied to a pressure of 500 MPa at 600°C for 1 hour through HP-HTS. In a previous investigation [17], we used HP-HTS to optimize the development of bulk $\text{Fe}(\text{Se},\text{Te})$, and the high superconducting characteristics could be attained by synthesizing the material at 600°C for an hour at 500 MPa. Table 1 includes a list of the prepared samples.

For the structural characterization of these samples, we have measured X-ray diffraction patterns using Rigaku SmartLab 3kW diffractometer with filtered $\text{Cu-K}\alpha$ radiation (wavelength: 1.5418 \AA , power: 30 mA, 40 kV), and a Dtex250 linear detector. A slow scan of the measurement profile from 5° to 70° with a very small step of $0.01^\circ/\text{min}$ was used to measure

our samples. Furthermore, ICDD PDF4+ 2021 standard diffraction patterns database and Rigaku's PDXL software were applied to perform the profile analysis. On the basis of these analyses, the quantitative values of impurity phases (%), and lattice parameters were calculated for various samples. Zeiss Ultra Plus field-emission scanning electron microscope equipped with the EDS microanalysis system by Bruker mod. Quantax 400 with an ultra-fast detector was carried out for the detailed macrostructural analysis and in the mapping of the constituent elements. Quantum Design PPMS attached to a vibrating sample magnetometer (VSM) was used to characterize the magnetic properties of these materials in the temperature range of 5-25 K and in the magnetic field up to 9 T. The magnetic susceptibility was measured in zero-field cooled (ZFC) and field-cooled modes at an applied magnetic field of 50 Oe with a slow temperature scan. The variation of resistivity with temperature was measured by a closed-cycle refrigerator (CCR) in a zero magnetic field with various current (5, 10, 20 mA), where all data were collected with a very slow warming process.

Results and discussion

The collected data of the powder X-ray diffraction patterns for various Gd-added $\text{FeSe}_{0.5}\text{Te}_{0.5}$ ($\text{FeSe}_{0.5}\text{Te}_{0.5} + x\text{Gd}$) samples are illustrated in Figure 1(a). All samples have the main tetragonal phase with the space group $P4/nmm$ as similar to the parent compound $\text{FeSe}_{0.5}\text{Te}_{0.5}$ ($x = 0$) [10]. The parent compound also has around 5-6% hexagonal phase as an impurity phase, which is well in agreement with the previous reports for 11 family [32, 10, 33]. Interestingly, a very small amount of Gd addition, such as 3% weight has reduced the hexagonal phase significantly, but a very small amount of Gd metal is also observed as a secondary phase. Furthermore, 5 wt% of Gd added sample shows almost no hexagonal phase and also no other impurity phase is observed. With the further addition of Gd, the hexagonal phase is completely suppressed and not observed again, however, the amount of the Gd metal as an impurity is increased with higher Gd additions, as listed in Table 2. Since Gd metal is very sensitive to air, so the sample having a high amount of Gd has also shown Gd_2O_3 impurity, which could be possible during the transfer of the powder XRD samples from the glove box. Since the sample with $x = 0.05$ has an almost clean pristine phase, we decided to grow the parent compound ($x = 0$) and 5 wt% of Gd added bulks ($x = 0.05$) by HP-HTS to understand the high pressure synthesis effects. In Figure 1(a), the parent sample ($x = 0_{\text{HIP}}$) and 5% weight Gd added sample ($x = 0.05_{\text{HIP}}$) prepared by HP-HTS are also shown. Interestingly, the parent compound, *i.e.*, $x = 0_{\text{HIP}}$, has almost the same amount of hexagonal phase as $x = 0$ sample obtained by CSP. Whereas the sample $x = 0.05$ prepared through HP-HTS have nearly no

hexagonal phase, a very small amount of GdSe phase is observed, as listed in Table 2. It suggests that the HP-HTS method somehow supports the formation of the GdTe/GdSe phase instead of the hexagonal phase under high-pressure growth of Gd added FeSe_{0.5}Te_{0.5}. Fitted XRD data for $x = 0, 0.05,$ and 0.05_HIP are shown in Figures 1(b), 1(c), and 1(d), where the experimentally observed and calculated intensity, and the difference between these two curves are depicted. The refinement is well fitted with a tetragonal phase with space group $P4/nmm$. As listed in Table 2, the lattice parameter of the parent compound prepared through CSP and HP-HTS has the lattice parameter ($a = 3.7950 \text{ \AA}, c = 5.9713 \text{ \AA}$) and ($a = 3.7976 \text{ \AA}, c = 5.9679 \text{ \AA}$) at ambient and applied pressure, respectively, as previously reported for polycrystalline samples ($a = 3.7909 \text{ \AA}, c = 5.9571 \text{ \AA}$) [11] and single crystals ($a = 3.815 \text{ \AA}, c = 6.069 \text{ \AA}$) of FeSe_{0.5}Te_{0.5} [34, 35, 36]. The lattice parameters and the qualitative values of the impurity phases of all samples are listed in Table 2. Interestingly, the hexagonal phase is reduced completely even with a small addition of Gd, which is similar to other metal additions such as Pb [27], Sn [18], Li [28], Ag [37], etc., but this hexagonal phase could not be reduced by the high-pressure synthesis method [17]. Data in Table 2 indicates the slight enhancement of lattice parameter ‘ c ’ with Gd additions with respect to the parent compound ($x = 0$), which suggests that Gd metal was somehow entered inside the tetragonal lattice of superconducting FeSe_{0.5}Te_{0.5} phase and Gd interstitial sites are along the c -axis, but it doesn’t change the amount of Se or Te concentrations. The effect of Gd addition is comparable to that of the earlier study based on Li doping in Fe(Se,Te) [28], where Li entered the superconducting lattice. Due to the presence of various impurity phases, there could be a slightly higher error in the refinement, especially for larger amounts of Gd additions. One important point is that, like other metal addition, Gd-addition promotes the formation of the tetragonal phase by reducing the hexagonal phase. However, Gd metal also manifests as an impurity phase, as listed in Table 2.

To analyse the actual composition of constituent elements and their distribution inside the sample, we have performed the elemental mapping and the energy dispersive X-ray (EDAX) which is shown in Figure 2. Data in Table 3 indicate the actual concentration of various elements from the EDAX analysis. The parent compound ($x = 0$) shows the homogeneous distribution of all elements, whereas 5% weight Gd addition (Figure 2(ii)) has the better homogeneous distribution of these elements compared to the parent compound (Figure 2(i)), which could be due to the reduced hexagonal phase. In very few places, we have observed Gd as a metal form. The inhomogeneity of these constituent elements is increased with the further addition of Gd. Figure 2(iii) shows the elemental mapping for the samples with

$x = 0.20$, where Gd metal is observed in many places with large areas, as discussed with XRD analysis. As shown in Figure 2, the parent compound exhibits a molar ratio of 1:0.49:0.51 (Fe:Se:Te), which is nearly identical to the bulks $\text{FeSe}_{0.5}\text{Te}_{0.5}$ with a small amount of Gd additions. As mentioned in Table 3, the nominal weight of the Gd addition is nearly equal to the actual concentration, but with a high number of Gd additions, the deviation in the molar ratio is slightly increased in comparison to that of the parent compound. These results indicate that Fe, Se, and Te concentrations are not affected by Gd additions, but non-uniform Gd distributions are clearly visible at high Gd addition levels.

Figures 3 (i) and 3(ii) show the mapping for the parent compound ($x = 0_{\text{HIP}}$) and Gd-added sample ($x = 0.05_{\text{HIP}}$) prepared using the HP-HTS technique. Figure 3(i) shows that the homogeneity of the various elements for $x = 0_{\text{HIP}}$ is the same as that of the parent compound prepared in ambient conditions (Figure 2(i)). Fe, Se, and Te are distributed relatively uniformly across the sample $x = 0.05_{\text{HIP}}$, but some regions are rich in Gd and Se elements, which points to the formation of the GdSe phase as proposed by the XRD study. This sample ($x = 0.05$) prepared at ambient pressure has a somewhat different mapping from this Gd-added sample ($x = 0.05_{\text{HIP}}$) (Figure 2(ii)). It implies that the homogeneity of the Gd and Se element distributions is decreased by the high-pressure effect. As shown in Table 3 and also by XRD analysis and mapping, HP-HTS for the Gd-added sample ($x = 0.05_{\text{HIP}}$) reduced the actual Se-content from the stoichiometry of $\text{FeSe}_{0.5}\text{Te}_{0.5}$ and produced an addition phase, GdSe. For these reasons, we have not prepared any other Gd added $\text{FeSe}_{0.5}\text{Te}_{0.5}$ bulks using HP-HTS.

In order to understand the microstructural analysis, the polycrystalline samples were polished manually using various sandpapers with different grades inside the glove box to collect backscattered scanning electron microscopy (BSE-SEM, revealing chemical contrast) images at different magnifications. Figure 4 depicts low to high-magnification images for three samples with $x = 0, 0.05$, and 0.2 . In these images, light gray, white, and black contrasts are observed corresponding to the phases of $\text{FeSe}_{0.5}\text{Te}_{0.5}$, Gd_2O_3 , and pores, respectively. Figure 4(a)–(c) demonstrates that the sample with $x = 0$ has two contrasts: light gray and black contrasts, and on the microscale, the microstructural images are nearly homogeneous. Numerous micropores as well as many well-connected, disk-shaped grains are observed. As illustrated in Figure 4(d)–(f), a minor addition of Gd ($x = 0.05$) tends to result in larger grains and slightly larger pores. Overall, the microstructural of the sample with $x = 0.05$ is almost identical to the parent compound. However, we have not observed Gd metal in these BSE images for $x = 0.05$, as previously noted via XRD and mapping. With further increasing

of Gd additions, it seems that grain size and pore size are increased. At higher amount of Gd additions, we have observed, the white contrasts related to Gd_2O_3 which confirmed the presence of Gd metals as an impurity phase, as similar to XRD analysis. Figures 4(h)-(j) depict the BSE images for the sample with $x = 0.20$, where a larger grain is observed with the enhanced pore size. As shown in Figure 4, white contrast (Gd_2O_3) is seen in more regions and bigger sections of the sample for Gd additions ($x > 0.05$), and the increased pore size is also noticeable. Because of the increased impurity phase (Gd_2O_3) between $FeSe_{0.5}Te_{0.5}$ grains, grain-to-grain connections are often drastically reduced, and intergranular supercurrent pathways are severely blocked. These investigations indicate that, in comparison to bulk samples with $x = 0$, Gd addition lowers the grain connections due to larger grain and pore sizes. As a result, it implies that neither grain connectivity nor material density have improved.

Figures 5 show BSE images for the parent compound ($x = 0$) and Gd-added sample ($x = 0.05_HIP$) prepared through HP-HTS techniques. Compared to the samples prepared through CSP (Figure 4), these samples are more compact. The sample $x = 0_HIP$ has several well-connected grains which reduces the size of the pores. The sample $x = 0.05_HIP$ also has better grain connections compared to the sample $x = 0.05$, but Gd_2O_3 or $GdSe$ is also observed as an impurity phase, which weakens the grain connections. The most prominent phase of Gd_2O_3 or $GdSe$ is randomly observed as a white contrast in the bulk sample at many places, such as inside grains and at grain boundaries, but the size of pores as a black contrast is smaller than in the samples with $x = 0.05$. These pores and impurity phases are what cause the samples' weak grain connections, and Figures 5(d)–(f) appear to show that the observed grains are disc-shaped. As reported for other iron-based superconductors [38, 39], we have not found any microcracks in our samples at the grain borders or within the grains. The sample density is found to be around 51%, 50%, 48%, 72%, and 56%, respectively, for $x = 0, 0.05, 0.07, 0.0_HIP,$ and 0.05_HIP , based on the theoretical density of $Fe(Se,Te)$ (6.99 g/cm^3) [11]. The small amount of Gd added sample, *i.e.*, $x = 0.05$, has almost the same density as that of the parent compound ($x = 0$). However, the HP-HTS method has slightly improved the density for the sample $x = 0.05_HIP$, whereas a large improvement is observed for the parent compound $x = 0_HIP$, as also demonstrated by the microstructural analysis. The microstructural analysis in Figures 4 and 5 reveals that the addition of Gd improves the grain size and increases the pore size, but that the sample density is almost identical to that of the parent compound ($x = 0$) regardless of whether samples are prepared using CSP or HP-HTS. A large amount of Gd additions degrades both the phase purity and the cleanliness of grain boundaries with large

pores. It is well known that non-superconducting phases at the grain boundaries create an obstacle to the superconducting properties, as reported for 1111 [38, 4], 122 [40], and also for the 11 family [41] [27]. As a result, our analysis suggests that even a very small amount of the rare earth addition to $\text{FeSe}_{0.5}\text{Te}_{0.5}$ is ineffective at boosting material density or enhancing grain size and connectivity.

To confirm the Meissner effect of these samples, the measured DC magnetic susceptibility ($\chi = 4\pi M/H$) is shown in Figure 6(a)-(b) for samples $x = 0$ and $x = 0.05$, $x = 0.0_{\text{HIP}}$, and $x = 0.05_{\text{HIP}}$ measured under an applied magnetic field of 50 Oe in the temperature range 5-20 K for zero-field-cooled (ZFC) and field-cooled (FC) magnetization curves. The normalized magnetic susceptibility was calculated and depicted in Figure 6(a)-(b) for a comparison, which confirms a bulk superconductivity for these samples. The parent compound ($x = 0$) shows a superconducting transition of 14 K and, 5% Gd added $\text{FeSe}_{0.5}\text{Te}_{0.5}$ ($x = 0.05$) has almost the same T_c as that of the parent compound. Also, ZFC and FC behaviour of these two samples is very similar, as depicted in Figure 6(a), which confirms that there is no change in Se or Te concentration inside the stoichiometry of $\text{FeSe}_{0.5}\text{Te}_{0.5}$, as also indicated by structural and microstructural analysis. Figure 6(b) shows the normalized magnetization behaviour for the bulk samples prepared by the HP-HTS method. The sample $x = 0_{\text{HIP}}$ has an enhanced onset transition temperature by 1.2 K with a sharper transition, suggesting a good grain connection. The sample $x = 0.05_{\text{HIP}}$ has a broader transition due to the presence of the impurity phase of GdSe but the onset transition is almost the same as that of $x = 0$. All bulk samples have depicted the single-step transition, suggesting the intergranular properties of these bulks are comparable to those reported for other families of FBS [42]. Therefore, these analyses also support the conclusion that Gd addition does not affect the superconducting transition of $\text{FeSe}_{0.5}\text{Te}_{0.5}$ whether it was prepared through CSP or HP-HTS, which is similar to what was found by microstructural analysis and XRD measurements. The almost same T_c value of the Gd added bulks prepared by CSP confirms that Gd does not change in Te/Se concentrations.

The variation of resistivity (ρ) with respect to the temperature is illustrated in Figure 7(a)-(c) for the nominal compositions of polycrystalline $\text{FeSe}_{0.5}\text{Te}_{0.5} + x\text{Gd}$ ($x = 0-0.2$) in a zero magnetic field prepared by CSP. Due to the structural phase transition, the parent $\text{FeSe}_{0.5}\text{Te}_{0.5}$ ($x = 0$) exhibits a large anomaly in resistivity at a temperature below ~ 110 K [16, 33]. The small amount of Gd addition, *i.e.*, $x = 0.03$, has enhanced the normal state resistivity, which might be possible due to the inhomogeneous distribution of a small amount of Gd

contents. However, the behaviour of the resistivity curve is very similar to that of the parent compound. With the further increase of Gd additions, the resistivity is reduced in a systematic way due to the increased concentration of Gd metallic element. Interestingly, the overall resistivity behaviour of all Gd-added samples up to 10 weight% ($x = 0.10$) has almost similar behaviour to the parent compound. The sample $x = 0.2$ has a completely different behaviour than the other samples, *i.e.*, metal to insulation behaviour, as shown in the inset of Figure 7(a). As discussed with XRD and microstructural analysis, this sample has the impurity phase of Gd_2O_3 , and this could be a reason for this metal to insulator behaviour. The low-temperature behaviours of these samples are depicted in Figure 7(b) in the temperature range from 5 K to 20 K, where all samples exhibit the superconducting transition. The parent compound displays a superconducting transition of 14.8 K but has a slightly broader transition. Interestingly, the low resistivity behaviour of these Gd-added samples is not very systematic. The sample with $x = 0.03$ has an onset T_c of 14 K and an offset T_c of 11.8 K, *i.e.*, transition width of 2.2 K. Further increase of Gd addition has marginally improved the transition width of 1.9 K for $x = 0.05$. The sample has an onset transition of 14.3 K and an offset transition of 12.4 K. In the next step, the sample with $x = 0.07$ has a T_c value of 13.1 K with an offset T_c of 9.81 K and a transition width (~ 3.3 K) almost similar to the parent compound. Interestingly, slightly higher Gd additions, *i.e.*, $x = 0.1$, show an onset T_c of 13.5 K and an offset T_c of 11.9 K with a transition width of 1.6 K. A large amount of Gd addition, *i.e.*, $x = 0.2$, has an onset transition of 12.7 K, but no zero resistivity is observed up to 7 K. It suggests that there is a non-superconducting phase inside the bulks, which is also confirmed by the XRD and microstructural analysis.

To comprehend the grain connections of these samples prepared through CSP, we have measured the temperature dependence of the resistivity under various currents ($I = 5, 10,$ and 20 mA). The individual grain effect, *i.e.*, the intragrain effect, is related to the onset transition temperature (T_c^{onset}), whereas the grain connections, *i.e.*, the intergrain effect, represent the offset transition temperature (T_c^{offset}) [43, 44]. These effects can be understood by the resistivity measurements under different applied currents. Figure 7(c) illustrates the resistivity behaviour in the low temperature region for these samples with three different currents $I = 5, 10,$ and 20 mA to investigate the grains and grain connectivity behaviours. The bulk sample with $x = 0.03$ has a broader transition with various currents where the onset and offset transitions are both sensitive with various currents, as shown in Figure 7(c). However, the samples with $x = 0.05$ and 0.07 have almost no transition broadening, which suggests good grain connections. The bulk samples with $x = 0.1$ have slightly broader transition and seem very similar to the parent

compound, which could be due to the enhanced impurity phase of Gd metal as seen in the XRD patterns. These analyses suggest that 5 to 7% weight of Gd addition has slightly improved the grain connections compared to the parent compound ($x = 0$) and other Gd-added samples. These findings corroborate the study of microstructural investigations that was previously described. Compared to our results with previous studies based on metal additions such as Sn and Pb added samples [18], the mid-range addition of Gd additions to $\text{FeSe}_{0.5}\text{Te}_{0.5}$ has almost no broadening of the transition with respect to the applied current, which suggests better grain connectivity but a lower superconducting transition due to the inhomogeneity of the bulks. Interestingly, Gd addition has a similar impact on the onset and offset of superconducting transitions. These results are well in agreement with microstructural and XRD analyses.

Figures 7(d) and 7(e) show the temperature dependence of resistivity behaviour for the $\text{FeSe}_{0.5}\text{Te}_{0.5}$ bulk prepared by the HP-HTS process for $x = 0_{\text{HIP}}$ and 0.05_{HIP} . In comparison to CSP, the resistivity of the parent compound ($x = 0$) has been reduced by almost 50% through HP-HTS, which might be due to improved sample density and proper grain connections, as discussed with the microstructural analysis [17]. In the case of 5 wt% of Gd addition, HP-HTS processes are not very effective due to the formation of the GdSe phase. Due to this impurity phase, the resistivity depicts the metal-to-insulation behaviour, which is almost identical to the sample $x = 0.2$. Figure 7(e) depicts the low-temperature behaviour of these samples: $x = 0$, 0_{HIP} , and 0.05_{HIP} . The sample $x = 0_{\text{HIP}}$ shows an enhanced transition temperature of 1.2 K, as also confirmed by the magnetization study, and the transition width is improved with respect to the sample $x = 0$. However, 5 wt% of Gd-added sample prepared by HP-HTS has an onset transition of 11.8 K, but the zero resistivity is not reached by the measured temperature range up to 7 K (Figure 7(e)). This behaviour, along with XRD and microstructural analysis, supports the existence of a non-superconducting phase and a decrease in Se contents in this sample.

To figure out the critical current density J_c , the magnetic hysteresis loops $M(H)$ at a constant temperature of 7 K were performed with the rectangular-shaped sample $x = 0$, 0.05 , and 0_{HIP} , 0.05_{HIP} . Similar to the previous reports for the parent $\text{Fe}(\text{Se},\text{Te})$ compounds [27, 45, 46], these samples depict the magnetic hysteresis loops under ferromagnetic effects due to the presence of a very tiny amount of iron, which is non-observable for the XRD measurements. The $M(H)$ loop for a sample with $x = 0_{\text{HIP}}$ is shown as an inset of Figure 8 after the subtraction of the normal state magnetization, *i.e.*, $M(H)$ loop at 22 K. In a similar way, Gd-added samples have also depicted the magnetic hysteresis loop with a large background. These measured M -

H loops enable for the calculation of the critical current properties of these samples, which is an important parameter from a practical point of view. The Bean model [47], which is popular and reliable for iron-based superconductors, is one of many models [48, 47] that have been proposed to obtain the J_c values. We have performed the J_c calculation by using the formula $J_c = 20\Delta m/Va(1-a/3b)$ [47], where Δm is the hysteresis loop width, V is the volume of the sample, and shorter and longer edges of the sample are a and b , respectively. The magnetic field dependence of the critical current density J_c for these samples is shown in Figure 8 at 7 K and for the measured magnetic field up to 9 T. The parent compound $x = 0$ has shown the maximum J_c values of the order of 10^2 A/cm² at 0 T which is almost similar to the previously reported paper on the basis of the CSP method [27]. The high-pressure synthesis of this sample, *i.e.*, $x = 0_{\text{HIP}}$, has shown the almost two orders of magnitude enhancement of J_c of the parent compound ($x = 0$), which is depicted in Figure 8. This J_c value of the order of 10^4 A/cm² is the highest value of FeSe_{0.5}Te_{0.5}, as reported by the melted synthesis route [49] or other methods [17]. Interestingly, 5 wt% of Gd added FeSe_{0.5}Te_{0.5} ($x = 0.05$) has the same J_c value and almost similar behaviour to the parent compound ($x = 0$), which could mean that this sample ($x = 0.05$) has the same sample density and the same microstructural likeness to the parent compound. High-pressure synthesis of the Gd added sample, *i.e.*, $x = 0.05_{\text{HIP}}$, has slightly improved J_c values than those of the parent compounds ($x = 0$) in the whole magnetic field range up to 9 T. The calculated J_c of all samples has similar behaviour. This J_c improvement of the sample $x = 0_{\text{HIP}}$ and 0.05_{HIP} might be due to improved grain connection and the improved sample density by the high-pressure growth method, as discussed above with microstructural analysis, which is capable of providing effective flux pinning centres. The same observation has also been also reported for MgB₂ [37] and NbTi- based superconductors [31], where Ag or Gd addition enhances J_c values due to extra pinning centres. One should note that 5 wt% of Gd-added bulks ($x = 0.05$) have almost the same J_c values [27], whereas Sn and Pb additions enhance the J_c values by one order of magnitudes by improving the intergranular current compared to other metal additions [30]. Sn metal additions also work well to improve and enhance the J_c values for Sn-added SmFeAs(O,F) [43]. These analyses suggest that Sn, Ag, or Pb, or cometal addition [20, 18] can be the most effective metal to enhance the J_c value for FeSe_{0.5}Te_{0.5} samples compared to the rare earth (Gd) addition. By using the calculated J_c values at 7 K, vortex pinning force density, F_p has been calculated by the formula $F_p = \mu_0 H \times J_c$ [50]. Similar to the previous studies [32, 46], the maximum F_p values of (~ 0.3 - 0.4 GN/m³) of the polycrystalline sample with $x = 0$ and $x = 0.05$ are nearly identical as those reported values

(~0.1-1 GN/m³) for Fe(Se,Te) bulks. The sample $x = 0.05_HIP$ has slightly higher F_p values (~0.6 GN/m³) than those of other samples ($x = 0$ and 0.05); which is in nice agreement with the J_c enhancement, as depicted in Figure 8. Curiously, the parent samples ($x = 0_HIP$) by HP-HTS have a significant increase in the maximum F_p value (~15 GN/cm³), supporting the high J_c values and improvement of pinning centres for this sample. These studies confirm that Gd additions are not improving the appropriate pinning centres in the direction of the enhancement of critical current properties, which can be concluded from the previous reports for Ag-added MgB₂ [37] and Sn-added other FBS bulk samples [43]. Even, high-pressure growth and high-pressure sintering are also not helpful for Gd-added Fe(Se,Te) bulks to further improve the J_c and F_p values.

To reach our finding based on our study, Figure 9 shows the variation of the lattice parameter ‘ c ’, transition temperature T_c^{onset} , the transition width (ΔT), room temperature resistivity (ρ_{300K}), and RRR (ρ_{300K}/ρ_{20K}) with respect to the weight concentration of Gd added FeSe_{0.5}Te_{0.5} samples (x). Interestingly, the lattice parameter ‘ c ’ is slightly increased with Gd addition, as shown in Figure 9(a), which suggests that a small amount of Gd enters the superconducting lattice either at Se sites or Te sites, however, some more detailed studies are needed in this direction. Even the HP-HTS process also enhanced the lattice ‘ c ’ for sample $x = 0.05_HIP$ which could be possible due to the reduced amount of Te/Se from the FeSe_{0.5}Te_{0.5} composition because this sample had GdSe as an impurity phase, as confirmed from XRD measurements. The T_c^{onset} is reduced with Gd addition in a systematic way, which suggests that Gd enters inside the tetragonal lattice and reduces the superconducting transition, as depicted in Figure 9(b). The parent compound through HP-HTS has enhanced the T_c around 1.2 K but 5 wt% Gd addition ($x = 0.05_HIP$) reduces the onset T_c due to the decreased Se-concentration. Figure 9(c) illustrates that the value of transition width ΔT ($= T_c^{onset} - T_c^{offset}$) is also suppressed with Gd addition and suggests the inhomogeneity of the sample which is supported by XRD and microstructural analysis. The room temperature resistivity (ρ_{300K}) is shown in Figure 9(d), and interestingly, is reduced with Gd addition due to the metallic nature of Gd. The sample with $x = 0.05_HIP$ has a higher resistivity than the sample with $x = 0.0_HIP$ due to the presence of GdSe phase. The residual resistivity ratio (RRR) of these samples is depicted in Figure 9(e), which decreased with Gd addition, even for the sample with $x = 0.05_HIP$, which suggests that homogeneity, grain connections, and phase purity of the samples are reduced with Gd addition prepared either through CSP or HP-HTS. All of the studies clearly specify that Gd addition is not an effective way to improve the superconducting properties of the 11 family. On the other

hand, adding a very small amount of Pb and Sn acts as an effective pinning centre [18] which increases the critical current density compared to the parent compound. This analysis suggests that rare earth Gd addition does not work as an effective method to improve both the superconducting properties and the intergranular properties.

Conclusion

The superconducting properties of FeSe_{0.5}Te_{0.5} bulks are explored with the rare earth Gd additions, for the first time, by the synthesis of a series of samples through CSP and HP-HTS. Structural analysis suggests that a small amount of Gd-addition entered the superconducting tetragonal lattice of FeSe_{0.5}Te_{0.5}, and due to this, the lattice parameter 'c' is increased systematically with these additions. Although the sample density of Gd added bulk is nearly identical to that of the parent compound whereas grain size, and pore size are increased with Gd addition, as proposed by the microstructural analysis. Furthermore, the superconducting transition T_c of Gd added FeSe_{0.5}Te_{0.5} bulks prepared either through CSP or HP-HTS is reduced with Gd additions, whereas J_c is almost the same as that of the parent compound through CSP but slightly improved by HP-HTS in the measured magnetic field up to 9 T due to the slightly enhanced sample density. Critical current analysis suggests that Gd addition is not suitable for providing additional pinning centres. HP-HTS processed FeSe_{0.5}Te_{0.5} bulks ($x = 0_{\text{HIP}}$) has improved the T_c value by 1.2 K and almost two order of magnitude of the J_c value. Our studies based on 11 family confirm that rare earth (Gd) additions cannot be a potential way to improve the intergrain connections, sample qualities, or superconducting properties of iron-based superconductors.

Acknowledgments:

The work was supported by SONATA-BIS 11 project (Registration number: 2021/42/E/ST5/00262) funded by National Science Centre (NCN), Poland. SJS acknowledges financial support from National Science Centre (NCN), Poland through research Project number: 2021/42/E/ST5/00262.

References

- [1] Y. Kamihara, T. Watanabe, M. Hirano, H. Hosono, "Iron-Based Layered Superconductor La[O_{1-x}Fx]FeAs (x = 0.05–0.12) with T_c = 26 K," *J. Am. Chem. Soc.*, vol. 130, p. 3296, 2008.
- [2] Bednorz, J. G., Müller, K. A. , "Possible highT_c superconductivity in the Ba–La–Cu–O system," *Zeitschrift für Physik B Condensed Matter*, vol. 64, pp. 189-193, 1986.
- [3] H. Hosono, A. Yamamoto, H. Hiramatsu and Y. Ma, "Recent advances in iron-based superconductors toward applications," *Materials Today*, vol. 21, no. 3, pp. 278-302, 2018.
- [4] S. J. Singh and M. Sturza, "Bulk and Single Crystal Growth Progress of Iron-Based Superconductors (FBS): 1111 and 1144," *Crystals*, vol. 12, p. 20, 2022.
- [5] S. J. Singh, P. Mele, "Future Potential of New High T_c Iron-Based Superconductors," in *Superconductivity*, Springer, 2020, pp. 243-268 (https://doi.org/10.1007/978-3-030-23303-7_9).
- [6] Y. Ma, "Progress in wire fabrication of iron-based superconductors," *Supercond. Sci. Technol.*, vol. 25, p. 113001, 2012.
- [7] Q. Si, R. Yu and E. Abrahams, "High-temperature superconductivity in iron pnictides and chalcogenides," *Nature Reviews Materials*, vol. 1, p. 16017, 2016.
- [8] S. J. Singh et al., "Transition Temperature and Upper Critical Field in SmFeAsO_{1-x}Fx Synthesized at Low Heating Temperatures," *IEEE Trans. Appl. Supercond.*, vol. 23, no. 3, p. 7300605, 2013.
- [9] S. Margadonna, Y. Takabayashi, Y. Ohishi, Y. Mizuguchi, Y. Takano, T. Kagayama, T. Nakagawa, M. Takata, and K. Prassides, "Pressure evolution of the low-temperature crystal structure and bonding of the superconductor FeSe," *Phys. Rev. B*, vol. 80, p. 064506, 2009.
- [10] Y. Takano and Y. Mizuguchi, "Review of Fe Chalcogenides as the Simplest Fe-Based Superconductor," *J. Phys. Soc. Jpn.*, vol. 79, p. 102001, 2010.
- [11] F.-C. Hsu, J.-Y. Luo, K.-W. Yeh, T.-K. Chen, T.-W. Huang, P. M. Wu, Y.-C. Lee, Y.-L. Huang, Y.-Y. Chu, D.-C. Yan, and M.-K. Wu, "Superconductivity in the PbO-type structure α -FeSe," *Proc. Natl. Acad. Sci. U. S. A.*, vol. 105, p. 14262, 2008.
- [12] A. Coldea, "Electronic Nematic States Tuned by Isoelectronic Substitution in Bulk FeSe_{1-x}S_x," *Front. Phys.*, vol. 8, p. 594500, 2021.
- [13] R. Viennois, E. Giannini, D. van der Marel, R. Černý, "Effect of Fe excess on structural, magnetic and superconducting properties of single-crystalline Fe_{1+x}Te_{1-y}Se_y," *Journal of Solid State Chemistry*, vol. 183, p. 769, 2010.
- [14] Z. Zajicek, S. J. Singh, H. Jones, P. Reiss, M. Bristow, A. Martin, A. Gower, A. McCollam, A. I. Coldea, "The drastic effect of the impurity scattering on the electronic and superconducting properties of Cu-doped FeSe," *Phys. Rev. B*, vol. 105, p. 115130, 2022.
- [15] Y. Mizuguchi, F. Tomioka, S. Tsuda, T. Yamaguchi and Y. Takano, "Substitution Effects on FeSe Superconductor," *J. Phys. Soc. Jpn.*, vol. 78, p. 074712, 2009.

- [16] Kuo-Wei Yeh et al., "Tellurium substitution effect on superconductivity of the α -phase iron selenide," *Europhysics Letters*, vol. 84, p. 37002, 2008.
- [17] M. Azam, M. Manasa et al., "High-Pressure Synthesis and the Enhancement of the Superconducting Properties of FeSe_{0.5}Te_{0.5}," *Materials*, vol. 16(15), p. 5358, 2023.
- [18] Manasa, M.; Azam, M.; Zajarniuk, T.; Diduszko, R.; Cetner, T.; Morawski, A.; Wiśniewski, A.; Singh, S. J., "Cometal Addition Effect on Superconducting Properties and Granular Behaviours of Polycrystalline FeSe_{0.5}Te_{0.5}," *Materials*, vol. 16, p. 2892, 2023.
- [19] D. F. Lee, X. Chaud and K. Salama, "Transport current density in bulk oriented-grained YBa₂Cu₃O_x/silver composites," *Physica C*, vol. 181, pp. 81-87, 1991.
- [20] M. R. Koblishka et al., "Excess Conductivity Analysis of Polycrystalline FeSe Samples with the Addition of Ag," *Materials*, vol. 13, p. 5018, 2020.
- [21] Y. Ma and X. Zhang, "Significantly enhanced critical current densities in MgB₂ tapes made by a scaleable nanocarbon addition route," *Appl. Phys. Lett.*, vol. 88, p. 072502, 2006.
- [22] D. M. Feldmann, T. G. Holesinger, R. Feenstra, D. C. Larbalestier, "A Review of the Influence of Grain Boundary Geometry on the Electromagnetic Properties of Polycrystalline YBa₂Cu₃O_{7-x} Films," *J. Am. Ceram. Soc.*, vol. 91, p. 1869, 2008.
- [23] T. Shibauchi, T. Hanaguri, Y. Matsuda, "Exotic Superconducting States in FeSe-based Materials," *J. Phys. Soc. Jpn.*, vol. 89, p. 102002, 2020.
- [24] H. Okamoto, "The Fe-Se (iron-selenium) system," *J. Phase Equilibria*, vol. 12, p. 383, 1991.
- [25] M.-H. Fang, H.-D. Wang, C.-H. Dong, Z.-J. Li, C.-M. Feng, J. Chen et al., "Fe-based superconductivity with T_c = 31 K bordering an antiferromagnetic insulator in (Ti,K)Fe_xSe₂," *Europhys. Lett.*, vol. 94, p. 27009, 2011.
- [26] Y. S. Manurung, K. Sebayang, A. Imaduddin, M. Sinambela, "Effect of KI Addition on FeSe Superconductors by Powder in Sealed Tube Method," *IOSR Journal of Applied Physics*, vol. 12, pp. 56-60, 2020.
- [27] Shiv J. Singh, Ryszard Diduszko, Przemysław Iwanowski, Tomasz Cetner, Andrzej Wisniewski, Andrzej Morawski, "Effect of Pb addition on microstructure, transport properties, and the critical current density in a polycrystalline FeSe_{0.5}Te_{0.5}," *Applied Physics A*, vol. 128, p. 476, 2022.
- [28] C.-M. Yang et al., "Enhancement of superconductivity in FeSe_{1-x}Te_x by Li doping," *Supercond. Sci. Technol.*, vol. 25, p. 095010, 2012.
- [29] M. Migita et al., "Substitution effects of Ag into FeSe_{0.5}Te_{0.5} superconductor," *Physica C: Superconductivity*, vol. 484, p. 66, 2013.
- [30] W. Li, J. Kang, S. Fu, Y. Hu, P. Hu, M. Zhu, Y. Li, "Rare earth doping effects on superconducting properties of MgB₂: A review," *Journal of Rare Earths*, vol. 37, pp. 124-133, 2019.
- [31] S. K. Ramjan, L. S. Sharath Chandra, Rashmi Singh, M. K. Chattopadhyay, "Effect of Gd addition on the superconducting properties of Ti-based V, Nb, Ta alloys," *Superconductivity*, vol. 6, p. 100048, 2023.

- [32] C. F. Zignani, G. De Marzi, V. Corato, A. Mancini, A. Vannozzi, A. Rufoloni, A. Leo, A. Guarino, A. Galluzzi, A. Nigro, M. Polichetti, A. della Corte, S. Pace, G. Grimaldi, "Improvements of high-field pinning properties of polycrystalline Fe(Se, Te) material by heat treatments," *J. Mater. Sci.*, vol. 54, p. 5092–5100, 2019.
- [33] B. C. Sales et al., "Bulk superconductivity at 14 K in single crystals of $\text{Fe}_{1+y}\text{Te}_x\text{Se}_{1-x}$," *Phys. Rev. B*, vol. 79, p. 094521, 2009.
- [34] Y. Mizuguchi et al., "Substitution Effects on FeSe Superconductor," *J. Phys. Soc. Jpn.*, vol. 78, p. 074712, 2009.
- [35] J. L. Her, Y. Kohama, Y. H. Matsuda, K. Kindo, W.-H. Yang, D. A. Chareev, E. S. Mitrofanova, O. S. Volkova, A. N. Vasiliev and J.-Y. Lin, "Anisotropy in the upper critical field of FeSe and $\text{FeSe}_{0.33}\text{Te}_{0.67}$ single crystals," *Supercond. Sci. Technol.*, vol. 28, p. 045013, 2015.
- [36] V. Tsurkan, J. Deisenhofer, A. Günther, Ch. Kant, H.-A. Krug von Nidda, F. Schrettle, A. Loidl, "Physical properties of $\text{FeSe}_{0.5}\text{Te}_{0.5}$ single crystals grown under different conditions," *Eur. Phys. J. B*, vol. 79, pp. 289-299, 2011.
- [37] C. Shekhar, R. Giri, R. S. Tiwari, O. N. Srivastava and S. K. Malik, "High critical current density and improved flux pinning in bulk MgB_2 synthesized by Ag addition," *Journal of Applied Physics*, vol. 101, p. 043906, 2007.
- [38] F. Kametani et al., "Combined microstructural and magneto optical study of current flow in Nd and Sm Fe-oxypnictides," *Supercond. Sci. Technol.*, vol. 22, p. 015010, 2009.
- [39] S. J. Singh et al., "Granular behavior observed in the polycrystalline superconducting LiFeAs ," *Supercond. Sci. Technol.*, vol. 28, p. 025006, 2015.
- [40] He Lin et al., "Effect of metal (Zn/In/Pb) additions on the microstructures and superconducting properties of $\text{Sr}_{1-x}\text{K}_x\text{Fe}_2\text{As}_2$ tapes," *Scripta Materialia*, vol. 112, p. 128, 2016.
- [41] N. Chen et al., "Enhancement of superconductivity in the sintered $\text{FeSe}_{0.5}\text{Te}_{0.5}$ bulks," *Journal of Alloys and Compounds*, vol. 633, p. 233–236, 2015.
- [42] Shiv J. Singh et al., "Significant enhancement of the intergrain coupling in lightly F-doped SmFeAsO superconductors," *Supercond. Sci. Technol.*, vol. 26, p. 065006, 2013.
- [43] S. J. Singh et al., "Enhancement of intergranular current density of Sm-based oxypnictide superconductors with Sn addition," *Supercond. Sci. Technol.*, vol. 27, p. 085010, 2014.
- [44] S. J. Singh et al., "Weak-link behaviour observed in iron-based superconductors with thick perovskite-type blocking layers," *Supercond. Sci. Technol.*, vol. 26, p. 105020, 2013.
- [45] Q. Nouailhetas, A. Koblishka-Veneva, M. R. Koblishka, P. Naik S., F. Schäfer, H. Ogino, C. Motz, K. Berger, B. Douine, Y. Slimani, and E. Hannachi, "Magnetic phases in superconducting, polycrystalline bulk FeSe samples," *AIP Advances*, vol. 11, p. 015230, 2021.
- [46] A. Galluzzi, K. Buchkov, V. Tomov, E. Nazarova, A. Leo, G. Grimaldi, M. Polichetti, "High Pinning Force Values of a Fe(Se, Te) Single Crystal Presenting a Second Magnetization Peak Phenomenon," *Materials*, vol. 14, p. 5214, 2021.

- [47] P.C. Bean et al., "Magnetization of high-field superconductors," *Rev. Mod. Phys.*, vol. 36, p. 31, 1985.
- [48] Anderson, P. W.; Kim, Y. B., "Hard Superconductivity: Theory of the Motion of Abrikosov Flux Lines," *Rev. Mod. Phys.* 36, 39, vol. 36, p. 39, 1964.
- [49] Masi, A.; Alvani, C.; Armenio, A. A.; Augieri, A.; Barba, L.; Campi, G.; Celentano, G.; Chita, G.; Fabbri, F.; Zignani, C. F.; Barbera, A. L.; Piperno, L.; Rizzo, F.; Rufoloni, A.; Silva, E.; Vannozzi, A.; and Varsano, F., "Fe(Se,Te) from melting routes: the influence of thermal processing on microstructure and superconducting properties," *Supercond. Sci. Technol.*, vol. 33, p. 084007, 2020.
- [50] D. Dew-Hughes, "Flux pinning mechanisms in type II superconductors," *Philos. Mag.*, vol. 30, pp. 293-305, 1974.

Table 1:

Details about the prepared $\text{FeSe}_{0.5}\text{Te}_{0.5} + x\text{Gd}$ samples and their synthesis conditions. CSP is used for “Conventional synthesis method at ambient pressure” and HP-HTS is used for “High gas pressure and high temperature synthesis method”.

Weight% of Gd addition	Sample code	Synthesis conditions	Growth method
0	$x = 0$	<i>First step:</i> heated at 600 °C, 11 h, 0 MPa ↓ <i>Second step:</i> heated at 600 °C, 4 h, 0 MPa	CSP
3%	$x = 0.03$	<i>First step:</i> heated at 600 °C, 11 h, 0 MPa ↓ <i>Second step:</i> Gd addition and heated at 600 °C, 4 h, 0 MPa	CSP
5%	$x = 0.05$	<i>First step:</i> heated at 600 °C, 11 h, 0 MPa ↓ <i>Second step:</i> Gd addition and heated at 600 °C, 4 h, 0 MPa	CSP
7%	$x = 0.07$	<i>First step:</i> heated at 600 °C, 11 h, 0 MPa ↓ <i>Second step:</i> Gd addition and heated at 600 °C, 4 h, 0 MPa	CSP
10%	$x = 0.1$	<i>First step:</i> heated at 600 °C, 11 h, 0 MPa ↓ <i>Second step:</i> Gd addition and heated at 600 °C, 4 h, 0 MPa	CSP
20%	$x = 0.20$	<i>First step:</i> heated at 600 °C, 11 h, 0 MPa ↓ <i>Second step:</i> Gd addition and heated at 600 °C, 4 h, 0 MPa	CSP
0	$x = 0_HIP$	<i>First step:</i> heated at 600 °C, 11 h, 0 MPa ↓ <i>Second step:</i> heated at 600 °C, 1 h, 500 MPa	HP-HTS
5%	$x = 0.05_HIP$	<i>First step:</i> heated at 600 °C, 11 h, 0 MPa ↓ <i>Second step:</i> Gd addition and heated at 600 °C, 1 h, 500 MPa	HP-HTS

Table 2:

A list of the calculated lattice parameters '*a*' and '*c*', and the impurity phases for FeSe_{0.5}Te_{0.5} + *x*Gd samples is provided. Rigaku's PDXL software and the ICDD PDF4+ 2021 standard diffraction patterns database have been used for the quantitative analysis of impurity phases (%) through the refinement of the measured XRD data.

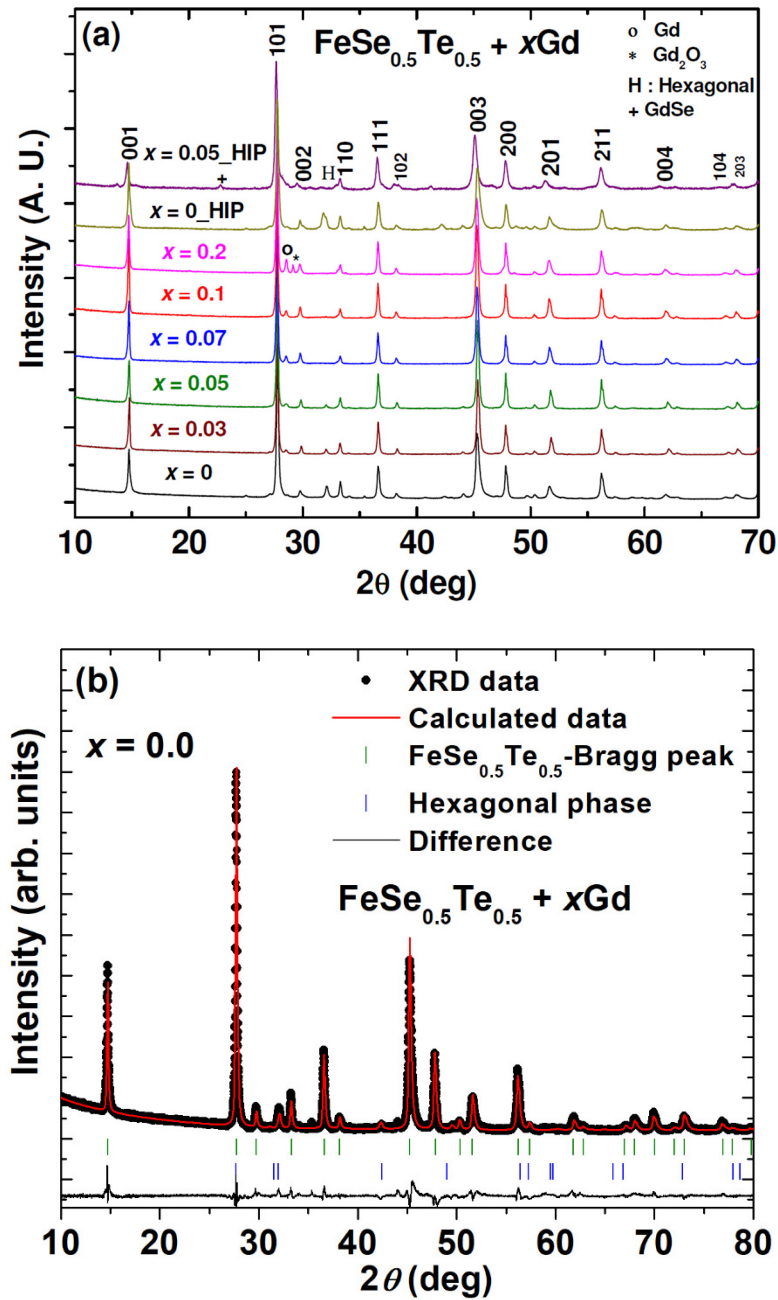
Sample (<i>x</i>)	Lattice ' <i>a</i> ' (Å)	Lattice ' <i>c</i> ' (Å)	Hexagonal phase (%)	Gd phase (%)	Gd ₂ O ₃ (%)	GdSe (%)
0	3.7950(1)	5.9713(3)	~5	-	-	-
0.03	3.7989(2)	5.9675(3)	~2	-	-	-
0.05	3.7983(8)	5.9744(2)	~1	-	-	-
0.07	3.7993(6)	5.9863(3)	-	~1-2	-	-
0.10	3.7993(9)	5.9892(4)	-	~2-3	-	-
0.20	3.7977(3)	5.9927(5)	-	~3	~2	-
0_HIP	3.7976(6)	5.9679(1)	~6	-	-	-
0.05_HIP	3.8047(2)	6.0463(4)	-	-	-	~3

Table 3:

List of the molar ratio of various elements presented in $\text{FeSe}_{0.5}\text{Te}_{0.5} + x\text{Gd}$ bulks.

Sample (x)	Fe Molar Ratio	Se Molar Ratio	Te Molar Ratio	Gd Molar Ratio
0	1	0.49	0.5	-
0.03	1	0.48	0.52	0.036
0.05	1	0.48	0.49	0.06
0.07	1	0.47	0.49	0.069
0.1	1	0.49	0.5	0.1
0.2	1	0.52	0.48	0.20
0_HIP	1	0.50	0.51	-
0.05_HIP	1	0.43	0.50	0.045

Figure 1: (a) X-ray diffraction patterns (XRD) of powdered $\text{FeSe}_{0.5}\text{Te}_{0.5} + x\text{Gd}$ ($x = 0, 0.03, 0.05, 0.07, 0.1$ and $0.2, 0_H\text{IP}, 0.05_H\text{IP}$) samples. The fitted XRD patterns with the experimental, calculated diffraction patterns and their differences at the room temperature are shown for the sample with (b) $x = 0$, (c) $x = 0.05$ (d) $x = 0.05_H\text{IP}$. Instead of the nominal composition of $\text{FeSe}_{0.5}\text{Te}_{0.5}$, the tetragonal phase of $\text{Fe}_{1.1}\text{Se}_{0.5}\text{Te}_{0.5}$ was observed as the real composition of the superconducting phase. One hexagonal phase, Fe_7Se_8 , has been found and is depicted as 'H' in figure (a). Table 1 contains a list of the obtained phases as well as the lattice parameters "a" and "c" that were obtained.



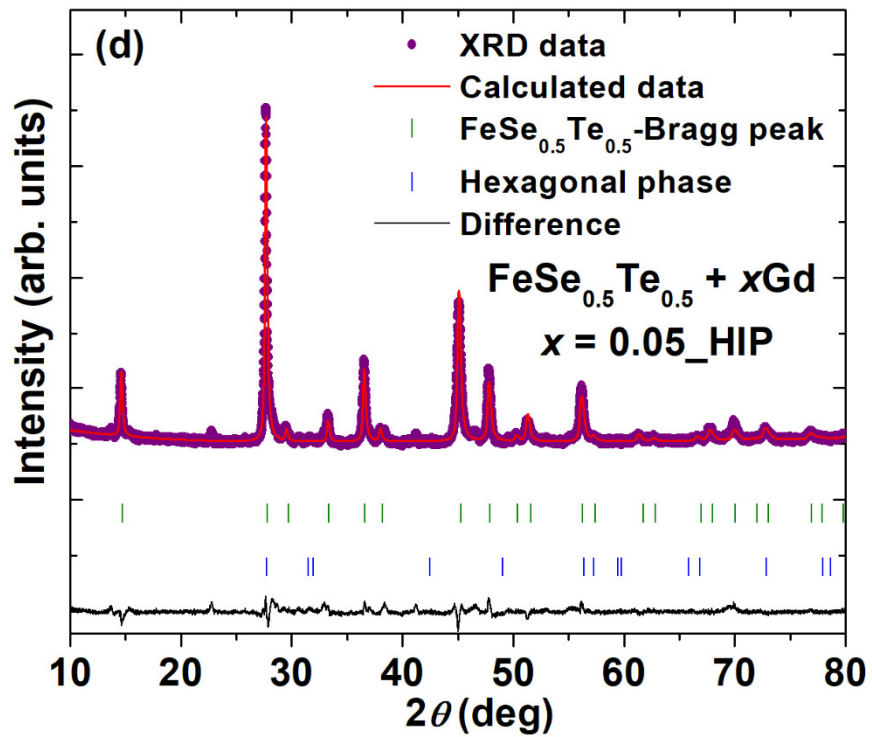
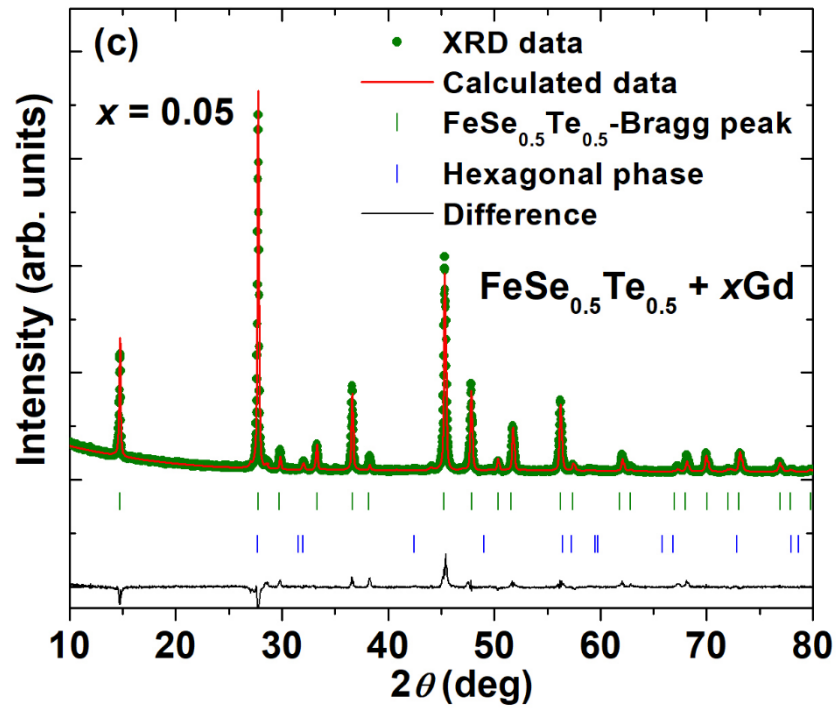


Figure 2: Mapping for the constituent elements of $\text{FeSe}_{0.5}\text{Te}_{0.5} + x\text{Gd}$ polycrystalline samples (i) the parent $x = 0$ (ii) $x = 0.05$ (iii) $x = 0.2$ prepared by CSP.

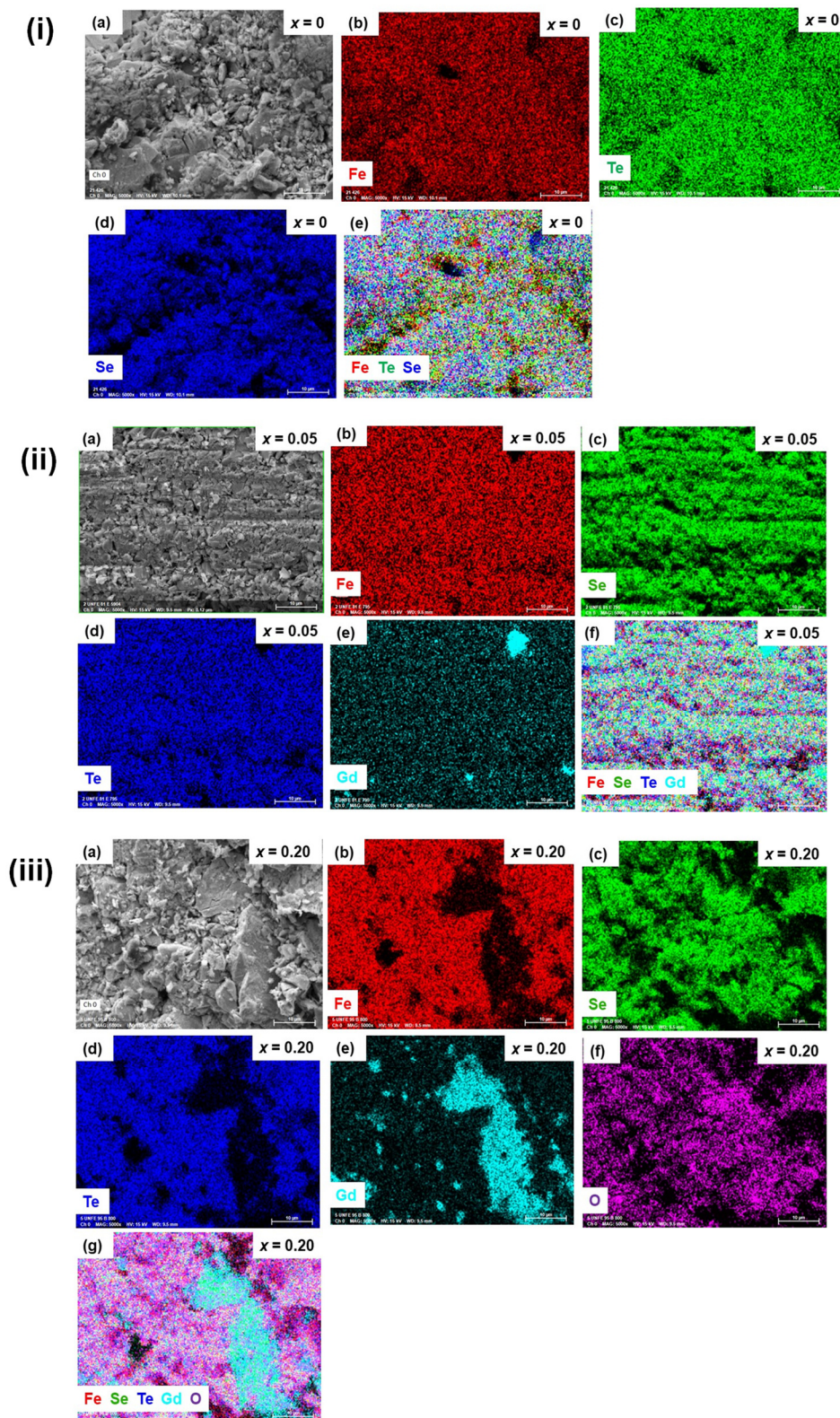


Figure 3: Mapping for the constituent elements of $\text{FeSe}_{0.5}\text{Te}_{0.5} + x\text{Gd}$ polycrystalline samples (i) the parent $x = 0_{\text{HIP}}$ (ii) $x = 0.05_{\text{HIP}}$ prepared by HP-HTS.

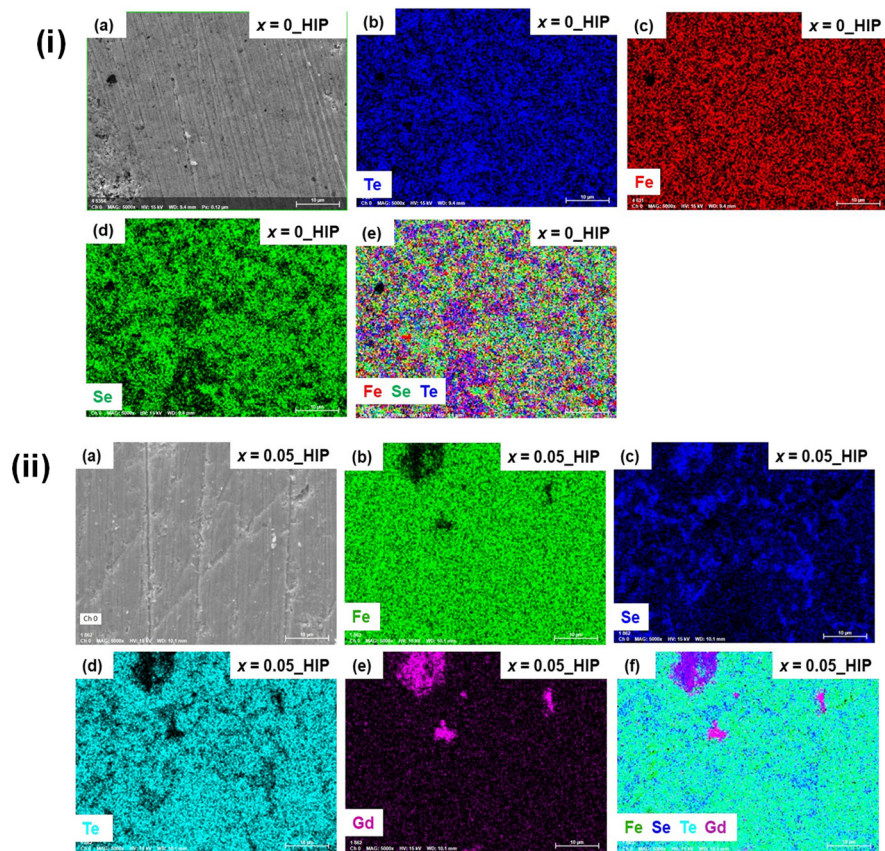


Figure 4: Back-scattered (BSE) images of $\text{FeSe}_{0.5}\text{Te}_{0.5} + x\text{Gd}$ polycrystalline samples: (a)-(c) for $x = 0$; (d)-(f) for $x = 0.05$; (g)-(i) for $x = 0.2$. Light gray, bright and black contrast correspond to $\text{FeSe}_{0.5}\text{Te}_{0.5}$, Gd_2O_3 , and pores, respectively

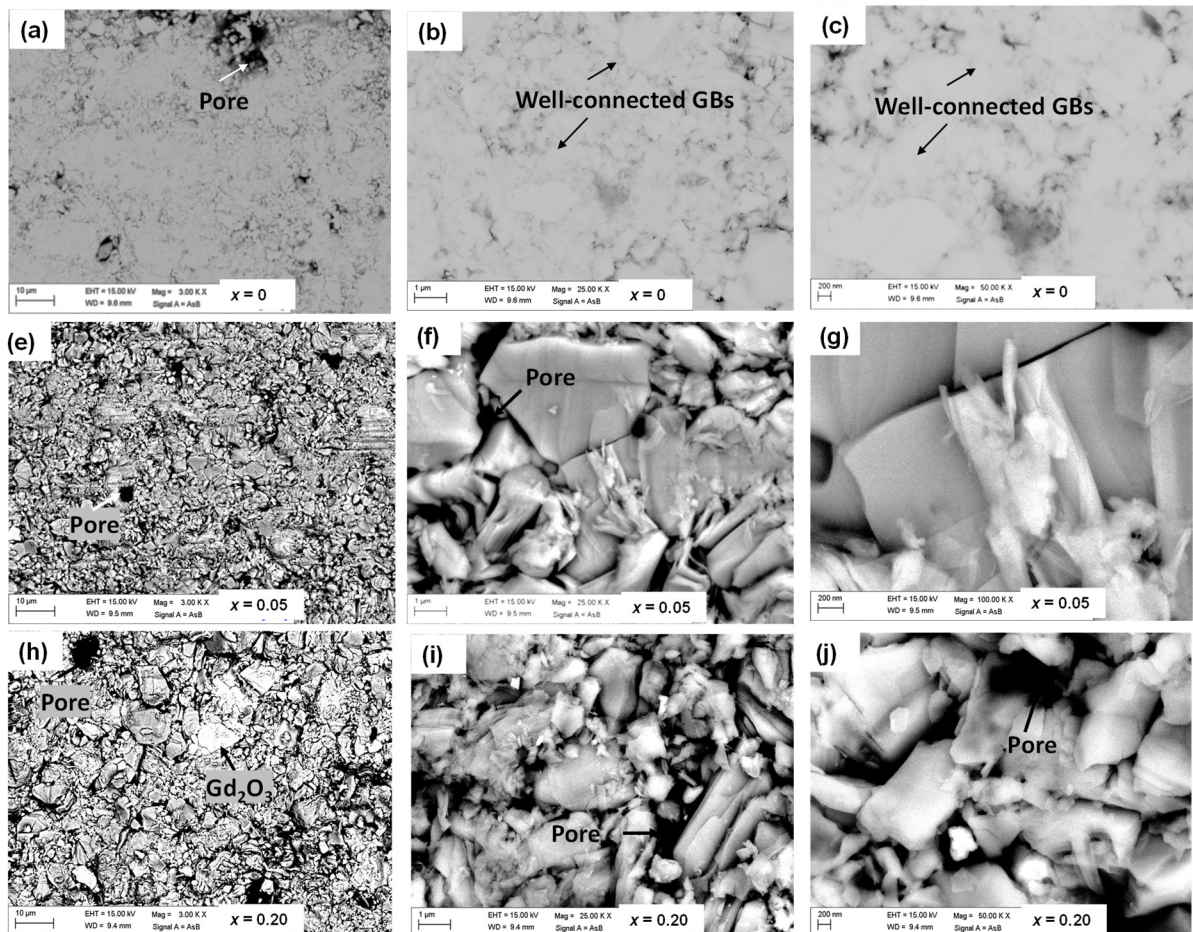


Figure 5: Back-scattered (BSE) images of $\text{FeSe}_{0.5}\text{Te}_{0.5} + x\text{Gd}$ polycrystalline samples: (a)-(c) for $x = 0_{\text{HIP}}$; (d)-(f) for $x = 0.05_{\text{HIP}}$ prepared by HP-HTS. Light gray, bright and black contrast correspond to $\text{FeSe}_{0.5}\text{Te}_{0.5}$, $\text{Gd}_2\text{O}_3/\text{GdSe}$, and pores, respectively.

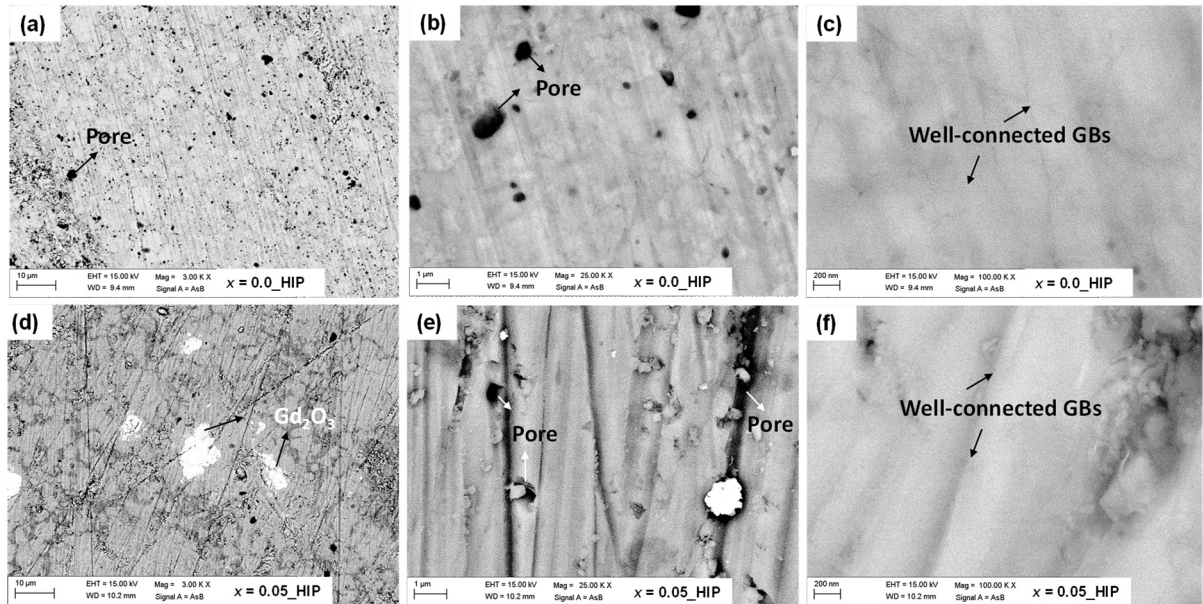


Figure 6: The temperature dependence of the magnetic susceptibility ($\chi = 4\pi M / H$) measured under zero field-cooled (ZFC) and field-cooled (FC) mode in an applied magnetic field $\mu_0 H = 20$ Oe for (a) $\text{FeSe}_{0.5}\text{Te}_{0.5} + x\text{Gd}$ ($x = 0$ and $x = 0.05$) bulks prepared by CSP and (b) $x = 0_{\text{HIP}}$, $x = 0.05_{\text{HIP}}$ prepared by HP-HTS.

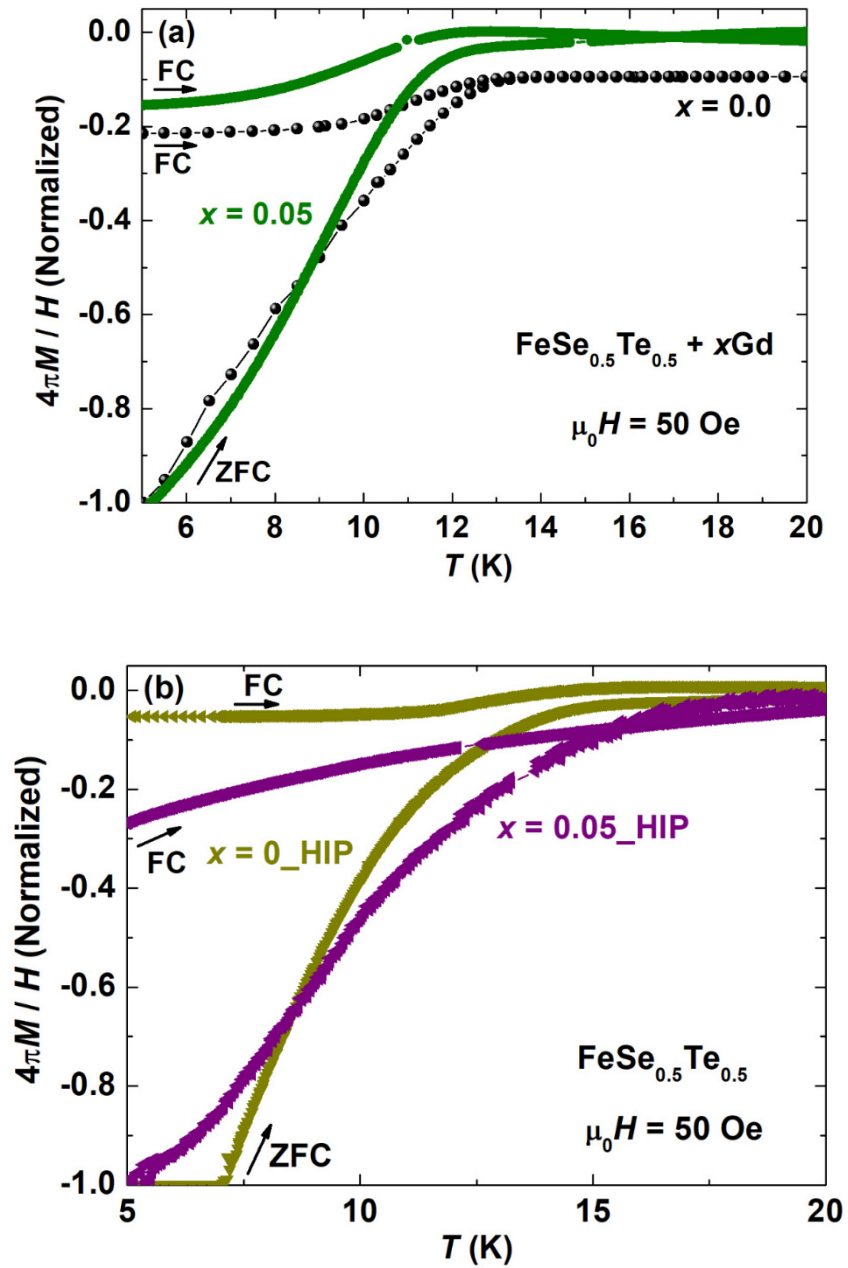
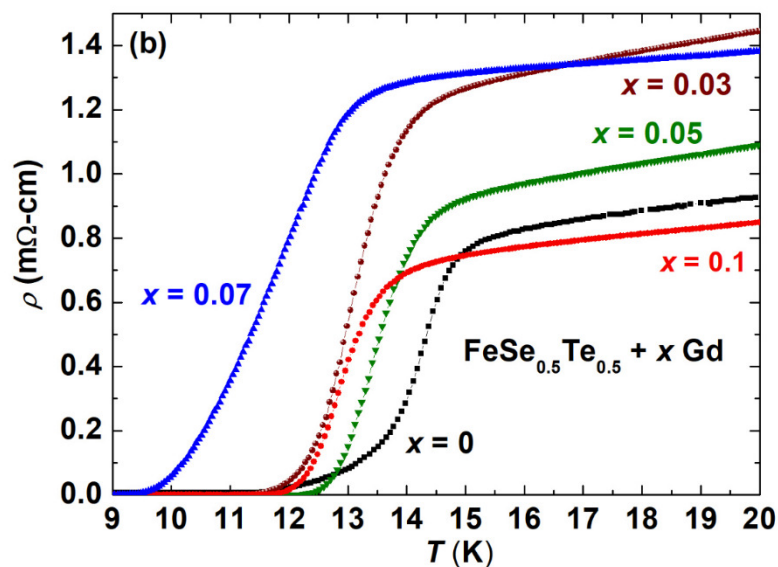
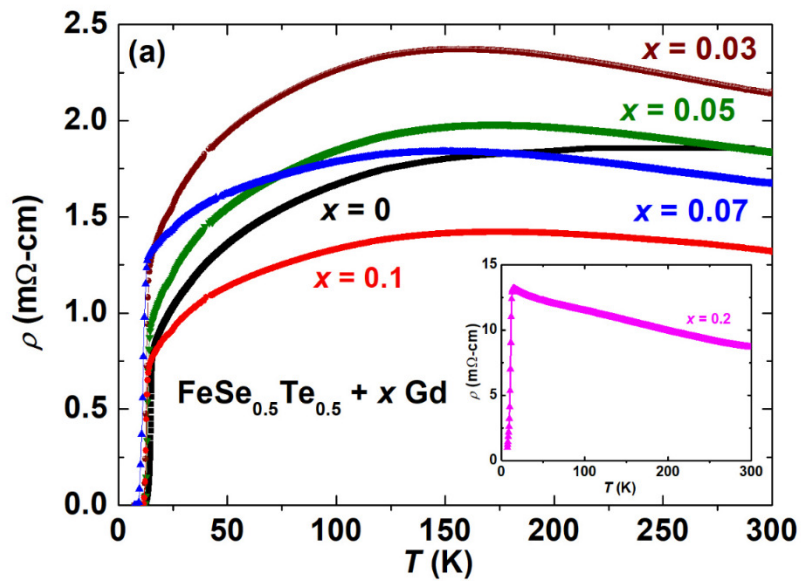


Figure 7: (a) The variation of resistivity (ρ) with the temperature for Gd added $\text{FeSe}_{0.5}\text{Te}_{0.5}$ ($\text{FeSe}_{0.5}\text{Te}_{0.5} + x\text{Gd}$ ($x = 0, 0.03, 0.05, 0.07, 0.10$) prepared by CSP. The inset shows the resistivity variation of the sample $x = 0.2$ in the whole temperature range. (b) Low temperature dependence of the resistivity behaviours for various samples prepared by CSP in low temperature region (9-20 K). (c) The temperature dependence of the low temperature resistivity for $\text{FeSe}_{0.5}\text{Te}_{0.5} + x\text{Gd}$ ($x = 0, 0.03, 0.05, 0.07, 0.10$) with respect to different currents $I = 5, 10, 20$ mA. (d) The temperature variation of resistivity in the whole temperature range and (e) Low temperature variation of resistivity for sample $x = 0.05_{\text{HIP}}$ and 0_{HIP} prepared by HP-HTS with the parent compound $x = 0$ prepared by CSP.



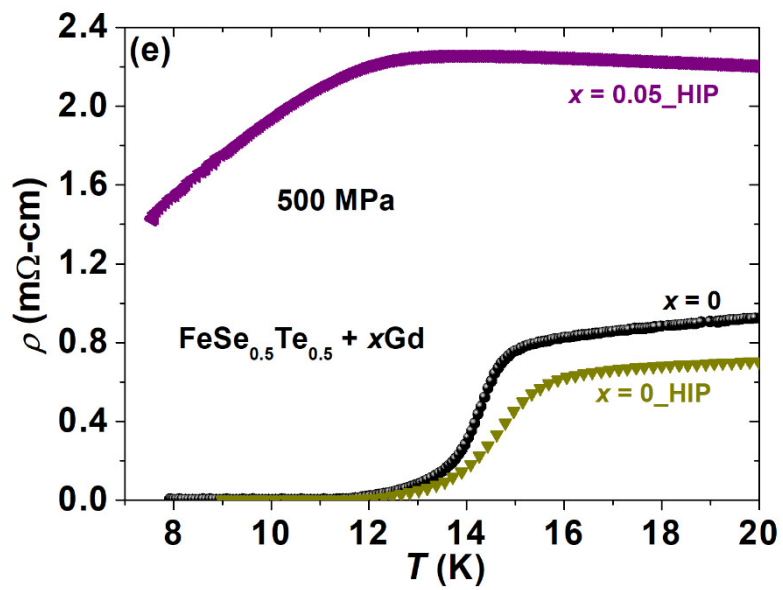
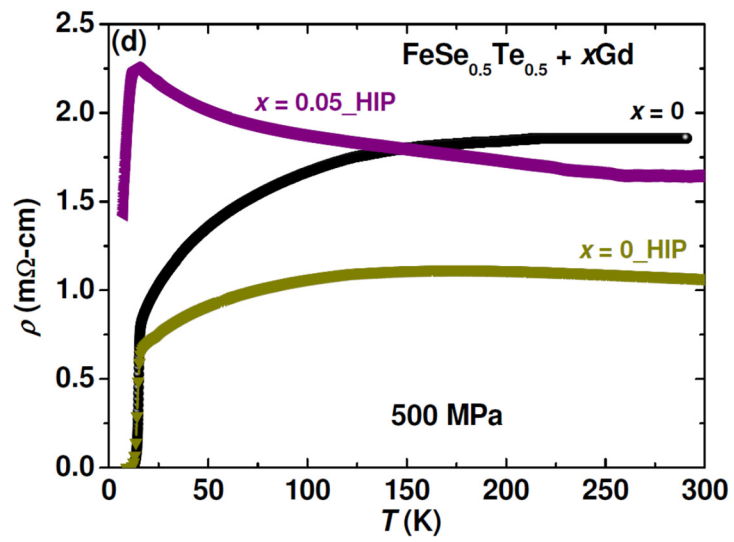
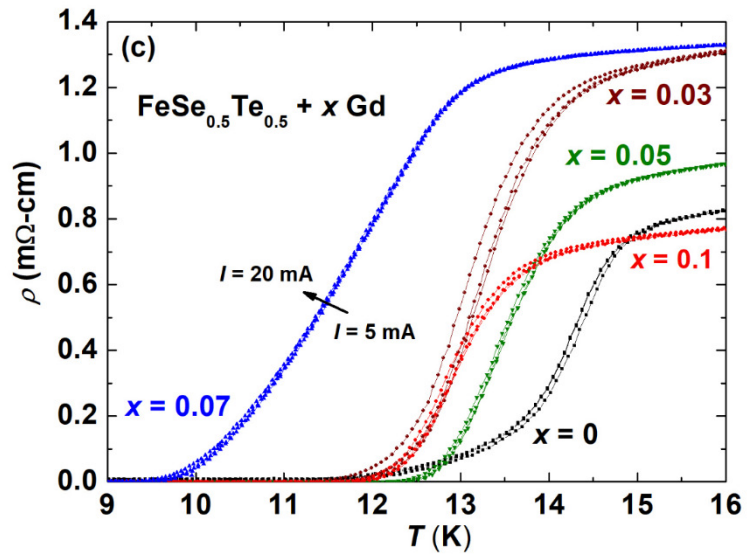


Figure 8: The critical current density (J_c) variation with the magnetic field (H) for $\text{FeSe}_{0.5}\text{Te}_{0.5} + x\text{Gd}$ ($x = 0, 0.05, 0.05_{\text{HIP}}$, and $x = 0_{\text{HIP}}$) samples up to 9 T at temperature of 7 K. The inset figure shows the magnetic hysteresis loop $M(H)$ at 7 K for $x = 0.0_{\text{HIP}}$ after the subtraction of the normal state background ($M(H)$ at 22 K).

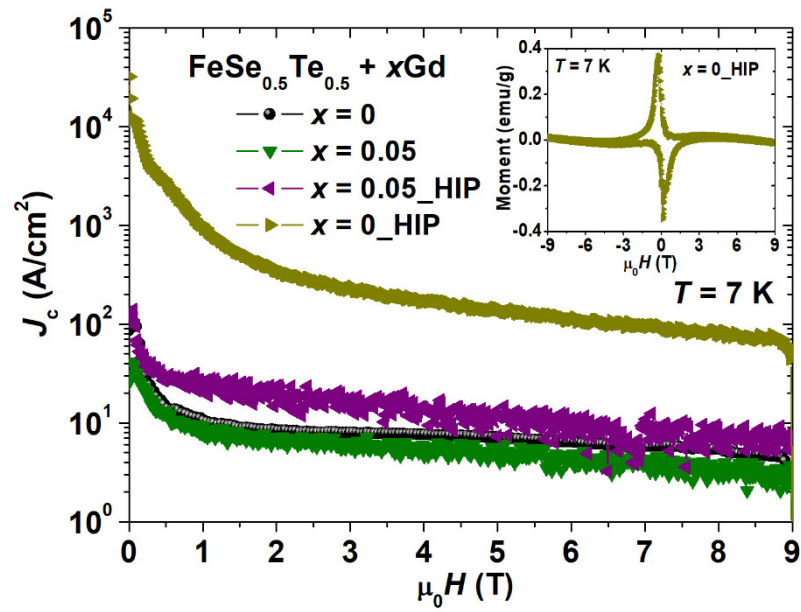


Figure 9: The variation of (a) lattice parameter 'c' (b) the onset transition temperature (T_c), (c) transition width (ΔT), (d) room temperature resistivity ρ_{300K} and (e) residual resistivity ratio RRR (ρ_{300K} / ρ_{20K}) with weight% of Gd addition for the parent $\text{FeSe}_{0.5}\text{Te}_{0.5}$ i.e. $\text{FeSe}_{0.5}\text{Te}_{0.5} + x\text{Gd}$ ($x = 0, 0.03, 0.05, 0.07, 0.1, \text{ and } 0.2$) prepared by CSP and HP-HTS.

